

## GEOCHEMISTRY

## Episodic reef growth in the Last Interglacial driven by competing influence of polar ice sheets to sea level rise

Karen Vyverberg<sup>1</sup>, Andrea Dutton<sup>1,2\*</sup>, Belinda Dechnik<sup>3</sup>, Jody M. Webster<sup>3</sup>, R. Lawrence Edwards<sup>4</sup>, Dan Zwartz<sup>5</sup>, Pu Zhang<sup>4</sup>, Mathieu Pythoud<sup>4</sup>, Robert M. DeConto<sup>6</sup>

Rapid, millennial-scale changes in sea level have been proposed for the beginning, middle, and/or end of the Last Interglacial (LIG) [~129 to 116 thousand years ago (ka)]. Each of these scenarios has different implications for polar ice sheet behavior in a warming world. Here, we present a suite of <sup>230</sup>Th ages for fossil corals in the Seychelles within a detailed sedimentary and stratigraphic context to evaluate the evolution of sea level during this past warm period. The rise to peak sea level at ~122 to 123 ka was punctuated by two abrupt stratigraphic discontinuities, defining three distinct generations of reef growth. We attribute the evidence of episodic reef growth and ephemeral sea-level fall to the competing influence of Northern Hemisphere ice melt and Antarctic ice regrowth. Asynchronous ice sheet contributions would mask the full extent of retreat for individual ice sheets during the LIG and imply greater temperature sensitivity of ice sheets than previously inferred.

## INTRODUCTION

The Last Interglacial (LIG) provides us with a window into the past to explore the stability of ice sheets and sea level when global mean temperatures were similar to those of today, and the polar regions were at least a few degrees Celsius warmer (1–7). Estimates of peak global mean sea level (GMSL) from far-field sites during the LIG range from 5.5 to 9 m above present (1, 8–10), while more recent reconstructions based on sites across the Bahamas platform suggest a lower peak between +1.2 to 5.3 m (11) or 0.4 to 2.7 m (12). The potential influence of the solid earth on vertical movements of the land surface (dynamic topography) casts additional uncertainty on the absolute magnitude of this peak (13). Those uncertainties notwithstanding, there is considerable independent evidence that both poles were warmer than present and that the Greenland ice sheet, and possibly the Antarctic, retreated relative to their modern configurations [see summary in (1)].

Establishing the absolute timing and rates of GMSL change during the LIG has the potential to reveal the dynamics of polar ice sheets in a warmer world and leads and lags within the climate system (e.g., relative to temperature, greenhouse gas concentrations, and solar insolation) that are pertinent to ongoing modeling efforts to project the magnitude and timing of future GMSL change [e.g., (14)]. Comparison of existing reconstructions reveals considerable debate regarding the timing, rate, and number of sea level peaks during the LIG sea level highstand (15–22). For example, the reported timing of peak sea level at individual localities ranges from ~122 to 114 ka (table S1). The stability of the Greenland ice sheet (GIS) and the Antarctic ice sheet (AIS) has also been questioned in response to numerous empirical sea level reconstructions that contain evidence for suborbital frequency oscillations in sea level within the LIG highstand (1, 15, 18, 20, 21, 23), while others have argued for a relatively stable sea level (11, 12, 24–26).

Shallow-water coral reefs are often used to reconstruct LIG sea level as they grow at or near sea level (27) and can be precisely dated using the <sup>230</sup>Th system (28). Fossil reefs that are far-field from the former ice-age Northern Hemisphere (NH) ice sheets are especially useful for LIG GMSL reconstructions as glacial isostatic adjustment (GIA) corrections are smaller and less sensitive to earth model parameters. The granitic Seychelles islands are a far-field site with respect to the margins of the Last Glacial Maximum ice sheets (8, 29, 30) and are considered tectonically stable since the Late Eocene based on the absence of any younger igneous intrusions (31). Previous work in the Seychelles provided a far-field estimate of the magnitude of peak sea level (9) and documentation of the sedimentary context for the radiometrically dated corals that we present here, including paleowater depth assessments of the corals as well as detailed sedimentary and stratigraphic analysis (32). Here, we provide 86 <sup>230</sup>Th ages from 24 individual fossil corals to establish the timing and rates of sea level change, in relation to concomitant changes in climate forcing and coral reef response.

## RESULTS

The geologic and sedimentary context of the limestone outcrops and the dated coral samples are briefly summarized here and described in detail elsewhere (9, 32). We studied limestone outcrops with in situ corals from the inner margin of the LIG reef, which represent the shallowest coral growth in the lagoon and resemble the morphology of modern reef deposits presently growing on granite bedrock that protrudes above the modern reef flat. The fossil corals sampled lived within a narrow paleowater depth range (0 to 2 m) that is inferred based on modern analogs of reef assemblages, providing a tight constraint on the position of past sea level (32). The outcrops contain a stratigraphically discontinuous succession, with episodes of reef accretion interrupted by sharp discontinuities that are variably covered by corals and lateral encrustations of the hydrozoan coral *Millepora exaesa* (Fig. 1). In two outcrops, there is convincing sedimentary (karstification and carbonate cement stratigraphy) and/or geochemical evidence (stable oxygen isotopes) of subaerial exposure, suggesting that the younger discontinuity resulted from a temporary drop in relative (local) sea level (RSL) (32).

<sup>1</sup>University of Florida, Gainesville, FL 32611, USA. <sup>2</sup>University of Wisconsin-Madison, Madison, WI 53706, USA. <sup>3</sup>Geocoastal Research Group, University of Sydney, Sydney, New South Wales 2006, Australia. <sup>4</sup>University of Minnesota, Minneapolis, MN 55455, USA. <sup>5</sup>Antarctic Research Centre, Victoria University of Wellington, Wellington 6012, New Zealand. <sup>6</sup>University of Massachusetts, Amherst, MA 01003, USA. \*Corresponding author. Email: dutton3@wisc.edu

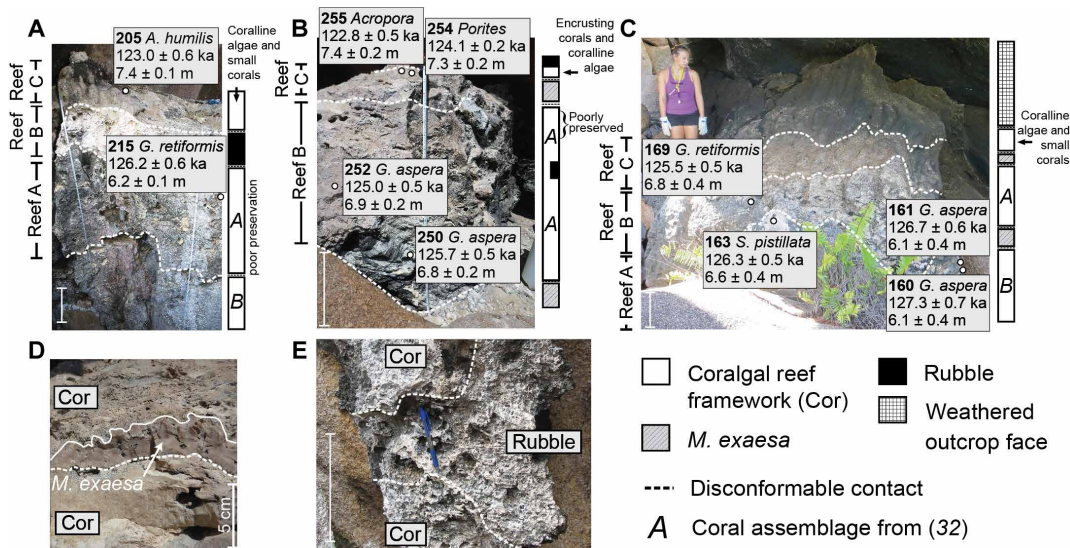


**Fig. 1. Outcrops with lithostratigraphic units, coral assemblages, sample locations and ages.** At (A) site 7, (B) site 11, and (C) site 33, episodes of reef growth defined by disconformities (dashed lines) capped by lateral encrustations of *M. exaesa* or coral rubble. White scale bars are 30 cm unless otherwise noted. Lithostratigraphic units are shown to the right of each photo where the italicized letters inside the box (A and B) refer to the coral assemblage (table S2). Panels (D) and (E) are examples of the two types of discontinuities observed in the outcrops. "Cor" denotes corals. Thin white line in (D) denotes top surface of *M. exaesa*. Photo in (A) is a splice of two separate photos. Photo credits: A. Dutton.

Corals in their original growth position from LIG fossil reef deposits on Curieuse and La Digue islands (fig. S1) were  $^{230}\text{Th}$ -dated in triplicate (see Materials and Methods). These data contribute 86 additional dates to the existing 68 high-precision dates from the Seychelles (9, 33), making it one of the most densely dated LIG sites in the world. The  $^{230}\text{Th}$  ages for each coral head (plotted as the inverse variance-weighted mean of multiple subsamples) reveal a trend of steadily decreasing age with increasing elevation (Fig. 2). Corals collected in protected caves (sites 8, 22A, and 32) plot below this trend, indicating that the caves represent a slightly deeper water environment than the remaining corals that were collected from exposed, seaward facing outcrops and define the rising sea level trend. Two corals collected by another field team (33) plot below the rising sea level trend; we were unable to independently verify their sedimentary context or primary growth position in the outcrop. We note that the rising sea level trend is reproduced by overlapping ages and elevations for each outcrop despite having to independently establish the vertical datum at each outcrop studied. This agreement provides multiple, independent sites of replication and also suggests that the corals sampled were living within a narrow paleowater depth window in the uppermost subtidal range, even narrower than our more conservative estimate of 0- to 2-m water depth (32). A trend of gradually rising GMSL during the LIG is also supported by other far-field data outside of the Seychelles region. For example, when corrected for GIA, coral U-Th data from both the Seychelles and Western Australia indicate a gradual rise in GMSL across the LIG from 129 to 122 ka, although the slope of the upward trend is sensitive to the GIA correction applied (see Materials and Methods and Supplementary Text) (Fig. 3).

## DISCUSSION

LIG corals recovered from emergent limestone outcrops in the Seychelles span a 6000-year time frame from  $128.7 \pm 0.5$  to  $122.8 \pm 0.5$  ka before present (B.P.), where present is 1950. Notably, this record

does not encompass the entire LIG GMSL highstand that is thought to have persisted for another 6000 years or so (26). We interpret that the most landward portions of the LIG reef that we have sampled represent the rise in RSL to its peak and that as RSL began to fall, the reef prograded offshore and has since been removed due to weathering and karstification during the last glacial cycle. Hence, our discussion is focused on reconstructing the sea level history from the 6000-year interval at the beginning of the LIG GMSL highstand.

## Timing of peak sea level

The two youngest ages,  $123.0 \pm 0.6$  and  $122.8 \pm 0.5$  ka B.P., are the same within reported uncertainties and represent the highest collected coral from each of two sites on opposite sides of La Digue Island (32). The highest corals in both outcrops display morphologies that are adapted to extremely limited accommodation (i.e., encrusters associated with the intertidal zone), providing a tight constraint on peak RSL at  $7.4 \pm 0.1$  m. Our observations are not consistent with the notion of a late, rapid peak in sea level during the LIG (17, 20) as there is no sedimentary evidence for later submergence of these shallow water corals. To the contrary, the uppermost coralgal facies in the outcrops studied indicates extremely limited vertical accommodation space and depositional characteristics associated with the uppermost subtidal to intertidal zone (32). Despite extensive reconnaissance on five islands, we did not find outcrops at higher elevations.

The timing of peak GMSL at  $\sim 122$  to 123 ka B.P. agrees with closed-system ages for the end of the main phase of reef growth at all of the other densely dated LIG reef sites (Western Australia, Barbados, and Bahamas) (Fig. 3) (26, 34, 35). Peak RSL in the Seychelles also appears to be coincident with the timing of maximum retreat of the GIS according to a suite of coupled ice sheet climate models and data from proximal marine cores (5, 36–39), which occurs several thousand years (kyr) after peak NH insolation at 127 ka B.P. (40). This lag in minimum ice volume relative to NH insolation is in apparent

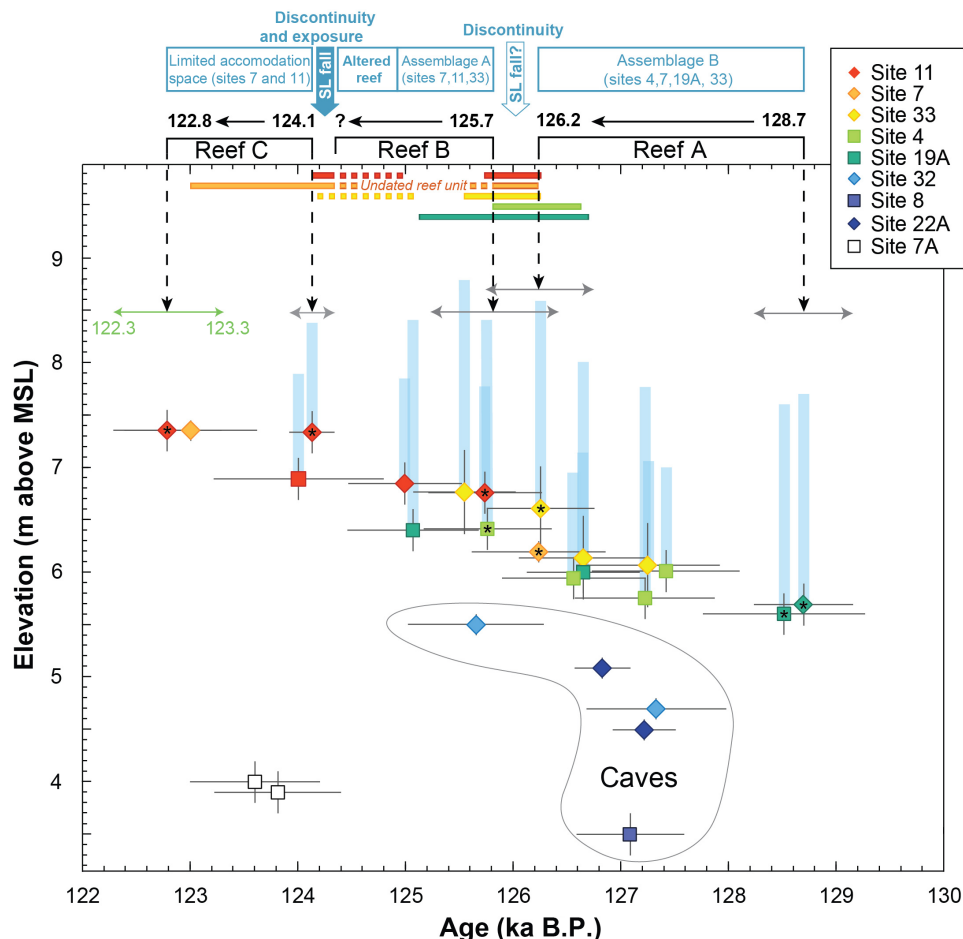


**Fig. 2. Age and elevation of fossil corals from the Seychelles.** Coral ages are shown with  $2\sigma$  uncertainties [diamonds, this study and squares from (9)]. Elevation error bars are  $1\sigma$  uncertainties, and paleowater depth range (translucent blue bars) is based on coral taxonomy, assemblage, stratigraphic context, and coral and outcrop morphology. Samples collected in caves represent a deeper coral facies (32). Open symbols indicate uncertain stratigraphic context for previously published data (33). Colored horizontal bars above the data correspond to site-specific hiatuses in reef growth associated with *M. exasea* or rubble layers bound stratigraphically by dated corals. Symbols with a black asterisk were used to calculate the timing of the base and top of each reef unit (table S4). Horizontal gray arrows denote the uncertainty on the bounding ages on reef growth.

agreement with the decade-old prediction by (41), but we note that the major inflection in rate of GMSL rise occurs at  $\sim 129$  ka BP, which demarcates the end of the main phase of deglacial sea level rise and the onset of the interglacial sea level highstand.

The estimated rate of GMSL rise averaged over the entire LIG Seychelles record ranges from  $0.29 \pm 0.03$  m/kyr to about 0.62 m/kyr (see Materials and Methods) depending on the assumed GIA contribution, which is an order of magnitude lower than contemporary rates of GMSL (42). The 1.7-m magnitude of GMSL rise observed across the interglacial agrees with the lower end of estimated GIS melt contributions (0.6 to 5.1 m) (1, 39, 43) but does not preclude the possibility of greater GIS melt that is partially offset by AIS growth as the NH warmed and the Southern Hemisphere cooled as the LIG progressed (44).

### Relative sea-level change captured by sedimentology and stratigraphy

The most intriguing observations arising from our Seychelles sea level reconstruction are provided by the pairing of our chronology

with a detailed sedimentologic analysis (32) revealing an episodic nature to reef growth (Fig. 2). While the age-elevation data taken alone suggest a steady increase in RSL from  $\sim 128$  to 123 ka BP, there are in fact three distinct episodes of reef growth (reefs A to C) punctuated by two abrupt discontinuities within this period (Fig. 2 and fig. S2). Using corals to bracket the timing of these interruptions to reef growth in each outcrop, we dated the first interruption in reef growth to  $\sim 126$  ka B.P. and the second to  $\sim 124$  ka B.P.

The first discontinuity between reefs A and B is observed as either a layer of coral rubble or an encrusting hydrozoan coral (*M. exasea*) that grew several centimeters thick but extends laterally over the entire reef A structure. Although coral rubble is not associated with a single environmental origin, *M. exasea* is known to encrust surfaces of dead coral (32). We were unable to find sedimentary evidence that pinpoints the precise cause for the demise of reef A (e.g., bleaching, disease, or sea level fall), but note that the sedimentary features of this discontinuity (coral rubble and encrustation by *M. exasea*) are identical to the discontinuity between reefs B and C. This younger discontinuity is associated with observational and geochemical evidence of an

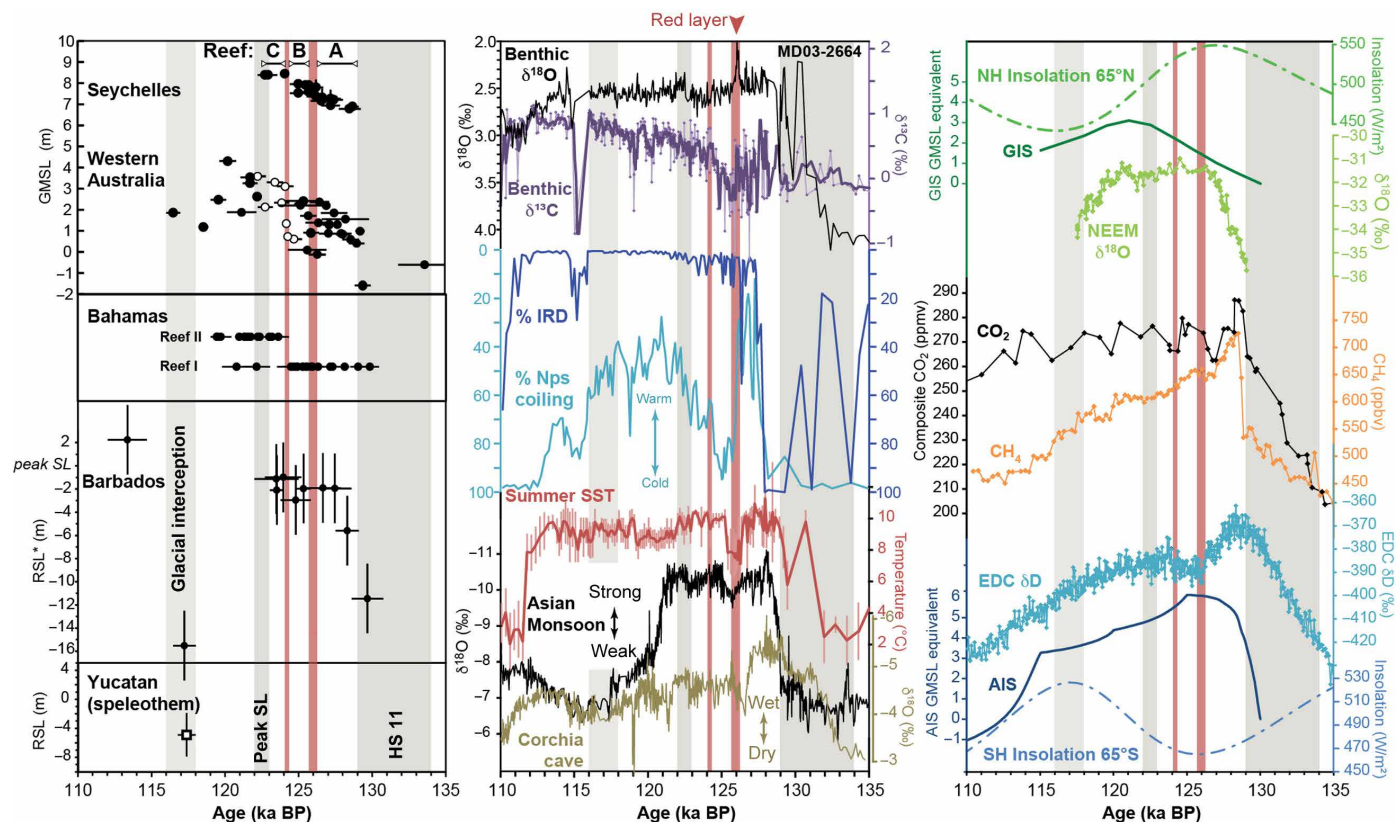


**Fig. 3. Comparison of sea level, North Atlantic proxies, speleothem, and ice core records.** Sea level data on left panel, top to bottom: Coral  $^{230}\text{Th}$  data for the shallowest corals from the Seychelles [this study and (9)], Western Australia and Barbados (84), and submerged speleothem  $^{230}\text{Th}$  from the Yucatan (69). The GIA correction introduces an additional vertical uncertainty, not shown here, to the datapoints from the Seychelles and Western Australia. Deep sea and speleothem data on middle panel, top to bottom: North Atlantic deep sea core MD03-2664 data (51, 60) on the Corchia cave timescale (52) for benthic  $\delta^{18}\text{O}$  and  $\delta^{13}\text{C}$ , % ice-rafted debris (IRD) and *Neogloboquadrina pachyderma* (sinistral) (Nps) coiling ratio, summer sea surface temperature (SST) estimate, Asian monsoon intensity (50), and speleothem  $\delta^{18}\text{O}$  for Corchia Cave denoting aridity (52). Timing of the red sediment layer (LIL0) in the Labrador Sea denoted by red arrow. Ice core data on right panel, top to bottom: NEEM ice core  $\delta^{18}\text{O}$  (5), Greenland synthetic temperature (85), and NH insolation (40), atmospheric  $\text{CO}_2$  (47) and  $\text{CH}_4$  (48), Epica Dome C (EDC)  $\delta\text{D}$  (4), and South Hemisphere insolation (40). Red vertical bars denote timing of discontinuities in the Seychelles reef section, and gray vertical bars are defined by labels in the left panel.

ephemeral sea level fall and subaerial exposure in the form of freshwater and marine carbonate cement stratigraphy and stable oxygen isotope analysis of these cements (32). Given the shared sedimentary characteristics with the similar disconformity up section, a brief subaerial exposure is also the most likely explanation for the discontinuity between reefs A and B.

In summary, the sedimentology and stratigraphy provide evidence for three distinct pulses of sea-level rise, punctuated by at least one (most likely, two) brief episode(s) of sea level fall. Because reefs are accretionary structures, they are better at recording intervals of sea level rise that create accommodation space for the reefs to accrete vertically, but it is more challenging to use them to capture the magnitude of falling sea level. In the case of the two disconformities, using our working hypothesis that they both represent episodes of brief sea level fall, they appear to have occurred quickly, e.g., sea level fall and subsequent rise occurring within an estimated 500 years for the discontinuity at  $\sim 126$  ka B.P. We note that the analytical uncertainties of the ages above and below the disconformity at  $\sim 126$  ka B.P. are overlapping, so the sea level oscillation is happening at a timescale that is finer than our chronological resolution based on the reported analytical uncertainties. However, we also

note that the accuracy of coral ages from different outcrops that mark the beginning and end of reef growth around this disconformity are remarkably reproducible, differing by a mere 21 to 22 years.

### Temporal progression of climate and reef stratigraphy

On the basis of previously published data and modeling studies summarized in the following discussion, we put forth a hypothesis that the episodic reef growth observed in the Seychelles reflects the competing influence of the growth and decay of ice sheets in the Northern versus Southern Hemispheres (Fig. 4). Several modeling studies suggest that the AIS contributed meltwater early in the LIG and then began to regrow as temperatures cooled in the Southern Ocean (14, 45, 46). In contrast, data and modeling studies of the GIS indicate that meltwater contributions peaked later in the LIG and that retreat to ice volumes smaller than the present configuration began after 127 ka, reaching maximum retreat around 121 to 122 ka B.P. before regrowing [e.g., (36, 37, 43)]. In the following, we detail evidence that leads us to conclude that reef A most likely grew in response to sea level rise driven by AIS retreat, whereas reefs B and C filled accommodation space created by meltwater contributions from the NH. Furthermore, we propose that the disconformities

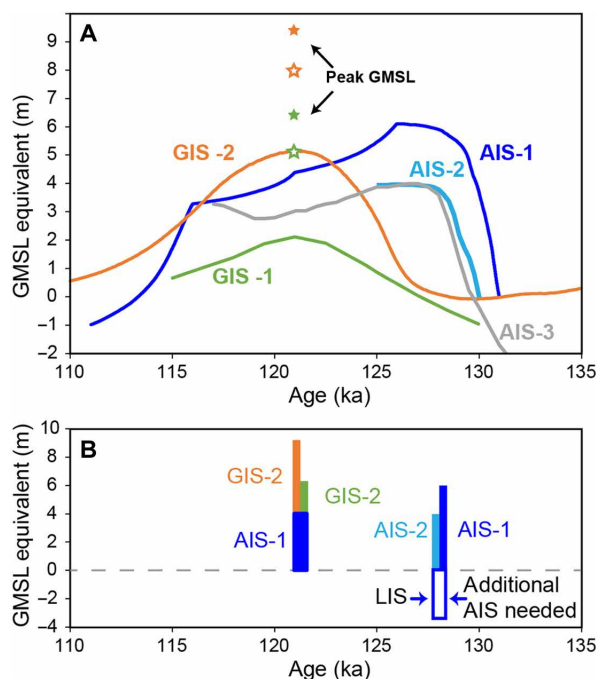


**Fig. 4. Phasing of ice sheet retreat in each hemisphere from ice sheet models and ice sheet budgets for two time slices.** (A) Early retreat of the Antarctic ice sheet [AIS-1 scenario b from (45), AIS-2 from (14), AIS-3 from (46)], two models showing later maximum retreat of the Greenland ice sheet, GIS-1 from (37) and GIS-2 from (38). Stars denote the timing and elevation of GMSL by adding the two GIS scenarios to the higher AIS-1 scenario (solid stars) and to AIS-3 (open stars). The total sum GMSL over time reflects the sometimes-competing influence of ice decay versus ice growth. Evolution of the LIS is not depicted but is inferred to supply an additional source of meltwater at ~126 ka B.P. (see Discussion). (B) Implied magnitude of individual ice sheet contributions from these transient ice sheet models early in the LIG and near the time of peak GMSL. As shown, any residual ice in the LIS early in the LIG (magnitude unknown) would have to be compensated by meltwater from another source such as the AIS to match the observed GMSL. Hence, even if GMSL was the same as present at ~129 ka B.P. (54), if there was a residual LIS present, then this must have been compensated with meltwater from another source.

both formed due to sea level drawdown as the AIS began to regrow. When rates of NH melting exceeded those of Southern Hemisphere ice growth, this created the accommodation space for reefs B and C to develop.

Reef growth in the Seychelles during the LIG initiates at  $128.7 \pm 0.5$  ka B.P. at nearly +6 m (all elevations relative to MSL) at the onset of the sea level highstand. We were unable to document the initial rise of sea level from 0 to +6 m because the corals at lower elevations have been eroded or geochemically and mineralogically altered by modern wave action and storm surges, making the corals we collected at lower elevations unsuitable for dating. The onset of the sea level highstand (reef A,  $128.7 \pm 0.5$  ka B.P.) is coincident with peaks and sharp transitions in ice cores [peak atmospheric  $\text{CO}_2$  (47) and  $\text{CH}_4$  (48) and Antarctic temperatures (4), abrupt shift in deuterium excess values, all at 128.5 to 128.7 ka] (49), the Asian Monsoon (transition at 128.9 ka) (50), and aligns with the onset of a brief interval of peak sea surface temperatures in the North Atlantic (51, 52). Hence, a wide variety of climate archives calibrated on several independent chronologies show a remarkably synchronous and abrupt, bi-hemispheric response.

Given indications that meltwater contributions from the GIS largely came later in the LIG, the rapid establishment of high elevation corals at the onset of the highstand was previously interpreted to reflect a contribution of meltwater from a sector of the AIS occurring within or at the end of the penultimate deglaciation (9). Several subsequent studies presented a variety of observational and modeling evidence for an early LIG meltwater contribution from the AIS. Early AIS retreat could have been driven by a bipolar see-saw response to the massive influx of freshwater into the North Atlantic during Heinrich event 11 (53) within the penultimate deglaciation. Ice sheet modeling studies of the AIS also suggests an early Antarctic contribution to sea level in the LIG (14, 45). Another study that used transient climate-ice sheet modeling of the AIS across the LIG suggested that the marine-based portion of the Eurasian ice sheet may have contributed to the rapid meltwater influx during H11 that increased subsurface warming that ultimately triggered some retreat of the AIS, although in that simulation the marine-ice sheet instability response in the AIS is delayed by a few kyr relative to the temperature forcing (54). An early LIG Antarctic meltwater contribution is also supported by the timing of the absence of ice in the Patriot Hills, Antarctica that is immediately preceded by a high abundance of methane-utilizing microbes, interpreted as resulting from subglacial methane hydrate destabilization due to ocean warming (55). In addition, an independent assessment of AIS volume changes across the LIG based on a comparison of seawater salinity in the North Atlantic with the Red Sea sea level reconstruction suggests AIS meltwater contributions early in the LIG that precede contributions from the GIS (18). Last, coastal archives in northern Europe and the UK also suggest an early contribution from Antarctica (56). Collectively, these studies lend weight to the interpretation that Antarctica contributed meltwater at or before the onset of the LIG sea level highstand.

Moving up section, the discontinuity that caps reef A is interpreted as most likely having formed due to an ephemeral sea level fall. Higher-than-modern temperatures are observed in Southern Ocean surface waters and peak temperatures are recorded by Antarctic ice cores in the first couple kyr of the LIG, from ~129 to 127 ka (4, 44). Subsequent cooling in the Southern Ocean and ice core records drives regrowth of ice in AIS in ice sheet models through the remainder of the LIG (14, 45). We hypothesize that AIS regrowth contributes to an ephemeral sea level fall in the far-field, including the Seychelles, where the magnitude of RSL fall would be slightly higher than that of GMSL fall owing to gravitational effects (29). Because the reef A corals were growing in extremely shallow water, even a small RSL fall of 1 m in the Seychelles may have been enough to subaerially expose the reef and cause the corals to die.

The base of reef B that overlies this disconformity marks the initiation of a major episode of reef growth in the Seychelles at  $125.7 \pm 0.5$  ka BP. We hypothesize that accommodation space for reef growth was provided in part by a pulse of meltwater in the North Atlantic derived from the disintegration of the Laurentide ice sheet (LIS), similar to the 8.2-kyr event in the Holocene when the LIS broke up into separate domes (57, 58). Meltwater from the GIS may have added to GMSL rise during this second interval of reef growth as well. The base of reef B at ~126 ka B.P. aligns temporally with widespread anomalies and abrupt transitions observed in North Atlantic climate and oceanography and ephemeral weakening of the Asian Monsoon and aridity in Europe (Fig. 3 and fig. S3) (50–52, 59, 60). While numerous multicentennial-scale climate and oceanographic anomalies have been documented during the LIG in

the North Atlantic (52), the most prominent of these occurs at ~126 ka BP and is well-characterized by data from deep sea core MD03-2664 from the Eirik Drift off the southern tip of Greenland that are shown plotted on an age model derived from aligning the pollen abundance off the Portugal margin with the U-Th dated Corchia Cave speleothem  $\delta^{18}\text{O}$  record (52). The higher climate variability in this region than during the Holocene has been attributed to incursions of meltwater from the GIS (52). Here, we propose that some of this variability was also driven by the LIS, the remnants of which may have persisted during the early LIG sea level highstand (58, 61).

At ~126 ka B.P., geochemical, sedimentary, and faunal proxies reveal a rapid southern expansion of the polar front, SST cooling of ~2°C, a spike in planktic foraminiferal Ba/Ca (signaling Ba-rich glacial meltwater), abruptly lower benthic  $\delta^{13}\text{C}$  values and deposition of a fine, red sediment layer (60). Sites proximal to East Greenland record a rapid pulse of meltwater discharge (freshening and cooling of surface waters) and subsurface warming (59). Together, this suite of proxies indicates a pulse of meltwater in the surface ocean in the North Atlantic, creating a freshwater lid that pushed the polar front to the south that resulted in contemporaneous aridity in Europe and a slight weakening of the Asian Monsoon.

The red sediment layer that is notably lacking in ice-rafted debris is ubiquitous in the Labrador Sea and has previously been interpreted as resulting from a Laurentide outburst flooding event similar to the Holocene 8.2-kyr event that is associated with the deterioration of the Laurentide and delivery of Hudson Bay-sourced sediments into the Labrador Sea (61). This event has been dubbed as the Last Inter-glacial Laurentide Outburst (LILO) in (58). Hence, we infer that the pulse of meltwater that initiates at ~126 ka was largely or partly derived from the LIS.

The resulting rise in GMSL due to meltwater emanating from the NH would have provided additional accommodation space for continued reef growth in the Seychelles (reef B), which is characterized by coral assemblages that are found in shallow (0 to 2 m) to intertidal water depths. At several sites, reef B is characterized by a monogeneric assemblage of *Goniastrea* sp., which likely represents an intertidal depth range (62). Hence, this assemblage reflects an extremely shallow-water environment and indicates that the reefs were able to keep up with this pulse in sea level rise as the reef accreted vertically. The magnitude of the rise in the Seychelles would have been greater than the global average by roughly 10 to 13% due to the sea level fingerprint of meltwater emanating from the GIS or LIS (29).

The 126-ka event marks the base of the reef B growth phase in the Seychelles, but unfortunately, the upper portion of Reef B is mineralogically altered (original coral aragonite has been partially converted to calcite), making it hard to date (Figs. 1 and 2). The surface of reef B at Grand Anse (site 11) is more heavily karstified than even the uppermost surface of any outcrop observed. This is noteworthy because the uppermost surface of the LIG outcrops has been exposed for the entire last glacial cycle. We hypothesize that lower solubility was promoted by the mixing of freshwater and seawater that would result from a small sea level fall at ~124 ka B.P. We also recovered a sequence of marine cement overlying a freshwater cement in the primary reef pore space in the upper portion of reef B at Anse Source d'Argent (site 7) (32). This combination of evidence leads us to interpret a temporary RSL fall that subaerially exposed the upper portion of Reef B, precipitating freshwater cements, promoting dissolution and karstification through the mixing of freshwater and seawater, and altering the coral skeletal mineralogy.

Because the dissolution and karstification immediately below this discontinuity is much greater than observed for the top of reef A, we infer that the magnitude of sea level fall was greater, more prolonged, or some combination of the two in comparison to the ephemeral sea level fall at ~126 ka. Reef B is terminated by an abrupt discontinuity and transitions up section into coral rubble or laterally encrusting *M. exasea*, depending on the outcrop. The end of this discontinuity (base of reef C) is dated to  $124.1 \pm 0.2$  ka B.P., but a bounding age on the end of reef B growth could not be determined owing to poor preservation.

The sedimentary evidence indicates that sea level fell at ~124 ka B.P., exposing the upper portion of reef B and developing the discontinuity between reefs B and C, at a time when models and data support ongoing retreat of the GIS [e.g., (5, 43)]. We interpret that the ephemeral sea level fall was driven by AIS regrowth that occurred in response to cooling Antarctic temperatures seen in ice cores and deep-sea cores (4, 44, 45). Hence, the episodic nature of reef growth is interpreted as the response to the competing influence of the growth and decay of the Antarctic, Greenland, and Laurentide ice sheets. This concept of asynchronous polar ice sheet contribution to sea level rise during the LIG has also been independently inferred using different methods (18). Although our results are in broad agreement with the notion of an early Antarctic contribution and later contributions of meltwater from Greenland as interpreted in (18), the details of the timing and large magnitude (~10 m) of sea level oscillations in their reconstruction differ from the Seychelles reef record that provides evidence for three successively higher peaks in GMSL within a radiometrically dated chronological framework (fig. S4).

A final phase of reef growth (reef C) caps this discontinuity but is limited to <20 cm of vertical growth, and all reef C corals observed exhibit morphologies that imply extremely limited accommodation space. At site 7, reef C is partially capped with a several-centimeter-thick, layered coralline algae deposit that would have accumulated in the intertidal to supratidal zone. This is interpreted to represent the last gasp of sea level rise and reef growth before sea level began to fall, eventually leading into glacial inception. This phase of sea level rise and reef growth was likely driven by melting from the GIS, given that maximum retreat of this ice sheet likely occurred at  $122 \pm 1$  ka (37–39, 43).

### Comparison to other LIG reef sites

Multiple (2–3), distinct generations of reef growth have been previously recognized at LIG sites around the globe, including the Bahamas (15), Barbados (63), Huon Peninsula (64), and the Yucatan Peninsula (19), among others [see summary in (18)]. Hence, the observation of episodic, multigenerational reef growth is not limited to the Seychelles but is a globally pervasive feature of LIG reefs. Open-system behavior in corals at all four of these other sites has made it challenging to pinpoint the precise timing of reef growth. To draw comparisons between sites, we restrict our analysis to closed-system ages only, which substantively reduces the size of some of the other datasets but incorporates only the best-preserved corals while simultaneously avoiding assumptions and uncertainties inherent in open-system models that are sometimes used to correct ages for altered corals.

The four most densely dated LIG fossil reefs are shown in Fig. 3. Maximum elevations of corals from the far-field sites of Western Australia and the Seychelles display stable to slowly rising (~0.3 m/kyr) RSL across the LIG and record a major phase of reef growth

from ~129 until about 122 to 123 ka. Far-field sites are characterized by a water loading signal from continental levering during the interglacial, which means that a stable to slightly rising RSL would be produced only if GMSL was rising during the LIG (Fig. 3 and figs. S5, S6) (65). While the rate of the rise is dependent on the particular GIA model applied, the conclusion that these two sites would require a net rise in GMSL across the LIG appears to be robust (see Materials and Methods and Supplementary Text). Hence, these two sites are consistent in terms of recording a similar timing for the main phase of reef growth and the overall pattern of GMSL rise across the LIG.

The timing of growth in Reef A at the Seychelles matches that observed at the southern sites in Western Australia (Foul Bay, Rottneest Island, and Shark Bay) and the landward (oldest) portion of the LIG terrace in Barbados (Fig. 3) (35). There is an extensive body of literature documenting an ephemeral sea level fall in the Bahamas during the LIG (15, 20, 23, 66, 67). Using closed-system ages from the two reef units defined in (23), the timing of the transition between these reef units aligns with the second discontinuity at ~124 ka B.P. (Fig. 3) (34). In Barbados, three LIG reef terraces plus one additional erosional, wave-cut platform that formed during a temporary sea level fall were described in (63). Their stratigraphy also places two episodes of reef growth (two terraces) before the wave-cut platform, followed by one additional episode of reef growth, matching the succession we have documented in the Seychelles. Two well-defined reef units have also been described at Xcaret, Mexico, but the precise timing of these reef units is uncertain due to poor preservation and lack of within-sample age reproducibility (19).

Discerning the magnitude and rates of the ephemeral GMSL fall and subsequent rise at ~124 ka is challenging, as there are no data from lower, more seaward outcrops in the Seychelles to capture the regression since they have been eroded through karstification and/or from wave action during the Holocene transgression. Notably, the sedimentary evidence in the Seychelles would not necessitate a sea level fall of  $\geq 4$  m and is therefore consistent with the findings in (24) that such large magnitude sea level oscillations did not occur.

Following the ephemeral sea level fall and rise at ~124 ka, a final episode of reef growth occurs until peak sea levels are reached between 122 and 123 ka B.P. Other global and regional studies have argued for a sea level highstand peak later in the LIG after 121 ka B.P. (19), perhaps at ~119 ka B.P. (17, 20). Despite extensive reconnaissance, no higher corals were found than those of ~122 to 123 ka B.P., and these do not show any evidence of later submergence, such as younger overgrowths. Instead, they indicate a sea level fall after ~122 to 123 ka BP, consistent with the falling sea level indicated by the data from Western Australia. The lagoon and back reef outcrops dated in the Seychelles represent the only LIG material remaining above current sea level in the Seychelles. Any seaward material (i.e., the reef crest, fore reef, etc.) has been eroded away, including any reef development during ephemeral drops in sea level or reef growth after ~122 ka B.P.

Our conclusion that there is no evidence for a late, rapid spike in sea level [e.g., (17, 20)] is not inconsistent with the observation of high elevation corals along the Quobba Ridge in Western Australia. The outcrops studied by (17) were surveyed in detail in another study and found to have a systematic, measurable change in elevation that mimics the folded bedrock in the region (68). These observations demonstrate that tectonic deformation has continued in the Quobba Ridge area (near Cape Cuvier) since the LIG period and

that the high corals observed are not a signal of a spike in GMSL, but rather of tectonic deformation.

The combination of coral age-elevation data from the Seychelles, Western Australia, and Barbados implies a gradual sea-level fall after ~122 ka BP that leads into a rapid glacial inception at or before ~117 ka as constrained by a  $^{230}\text{Th}$ -dated submerged (–4.9 m) speleothem from the Yucatan that initiated growth after subaerial exposure (Fig. 3) (69). Although the Bahamas dataset has some ages that extend younger than 122 ka B.P., this is consistent with GIA modeling that predicts a later peak in RSL at sites sitting on the peripheral bulge of the LIS [e.g., (8)] for a scenario where GMSL starts to fall before rapid glacial inception, so it does not change our interpretation of the timing of peak GMSL.

### Implications for dynamic behavior of polar ice sheets

We have documented the timing of three distinct episodes of reef growth in the Seychelles that are consistent with observations at other LIG reef sites around the globe. These three reef units are punctuated by two disconformities at ~126 and 124 ka B.P., both of which may reflect an ephemeral sea level fall followed by a rapid rise. These observations are consistent with an early collapse of a sector of the AIS at or before ~129 ka B.P. followed by regrowth superimposed upon episodic meltwater input into the North Atlantic from the LIS and/or GIS. This out-of-phase behavior of the ice sheets in the Northern and Southern Hemisphere is consistent with ice sheet models of the Antarctic and Greenland ice sheets during the LIG (Fig. 4). These ice sheet models are consistent with, and in some cases forced by, paleotemperature reconstructions that indicate peak temperatures early in the LIG in the Antarctic region and later in the LIG in the Arctic [e.g., (44)].

The scenario of some Laurentide ice persisting into the LIG until about 126 ka B.P. has been previously proposed by several authors based on independent assessments of sedimentological evidence paired with age models constructed using orbital and paleomagnetic approaches (51, 58, 61). The red sediment observed in Labrador Sea cores is similar to the sediment observed in the Holocene portion during the 8.2-kyr event that is thought to derive from the Hudson Bay region and represent the final deterioration of the LIS. The timing of the 8.2-kyr event in the Holocene is about 11 kyr after the beginning of the deglaciation [~19 ka (70)] and the L1LO event at ~126 ka B.P. is 11 kyr after 137 ka B.P., which is the approximate time that the penultimate deglaciation is thought to have commenced (71). Hence, because termination II (TII, the penultimate deglaciation) leading into the LIG occurred over a more compressed time frame than termination I (71), it is perhaps expected that some portion of the LIS persisted for a few thousand years into the LIG.

The state of the cryosphere during the LIG, with retreat implied in both Antarctica and Greenland as well as the total loss of the LIS (72), stands out relative to other Quaternary interglacials that had similar atmospheric  $\text{CO}_2$  levels but lower GMSL. Recent evidence from cosmogenic nuclide data also suggests that the LIG was anomalous given that the LIS was more persistent than not during Quaternary interglacials (73). Although this conundrum is yet to be solved, one possibility is that the retreat of ice during the LIG stems not directly from climate forcing during the interglacial itself but rather is a by-product of a particularly rapid deglaciation during TII. This was proposed by (54) who used a transient simulation to show that a longer interval of Atlantic Meridional Overturning Circulation (AMOC) reduction induced by Heinrich event 11 (H11)

during TII caused subsurface warming that contributed to excess loss from the GIS and AIS during the LIG. That study pointed to the marine-based portion of the Eurasian Ice Sheet that had a greater extent during MIS 6 than during the LGM as the trigger for rapid sea level rise and an extended period of AMOC reduction. Another study also invoked subsurface warming at high southern latitudes during H11 due to a bipolar seesaw effect to explain AIS retreat to a smaller-than-modern configuration (53). What neither of these studies was able to explore, due to the lack of a fully coupled ice-ocean-atmosphere model, is how Antarctic meltwater early in the LIG may have created feedbacks on the behavior of ice sheets in both hemispheres for the duration of the LIG. In general, while partial retreat of the ice sheet in Greenland has long been explained as a response to higher boreal insolation forcing during the LIG in comparison to the present interglacial, the proximal cause of AIS retreat has remained more enigmatic. Additional studies exploring the interplay of ice sheets, oceans, and atmosphere during TII and into the LIG are needed to further unpack the mechanisms and tipping points leading to polar ice sheet retreat.

Notably, the scenario we propose suggests that peak contributions from the AIS and GIS are not coincident, meaning that the budget of contributions at peak GMSL at 122 to 123 ka B.P. may require a larger contribution from the GIS (>2 m) to offset ongoing regrowth of the AIS. Likewise, the GMSL budget at the onset of the highstand would have incorporated some residual Laurentide ice in addition to the Antarctic meltwater contribution, meaning that this could imply an even larger AIS retreat to compensate for the remaining grounded ice volume in the Laurentide (Fig. 4B). Although the West Antarctic Ice Sheet (WAIS) is generally viewed as the most vulnerable to collapse, to compensate for remaining ice on North America in the early LIG and still explain our observations in the Seychelles would seem to require additional ice from Antarctica. This raises the possibility that marine-based sectors in East Antarctica may have become destabilized during the transition into the LIG sea level highstand, consistent with recent inferences of thinning, melting, and possible retreat in the Wilkes subglacial basin (74). While there are multiple scenarios of ice sheet histories across the LIG that might equally satisfy our observations in the far field, chronological constraints on climatic anomalies in the North Atlantic and their influence on the Asian Monsoon lend additional support to our interpretation that the abrupt, suborbital meltwater pulses that provided accommodation space for reef growth were associated with stepwise contribution of meltwater at high northern latitudes. Moreover, the rapid nature of these sea level oscillations points to the potential for stepwise pulses in ice sheet retreat that punctuate a more gradual, background rate of melting.

Our results provide observational constraints for future modeling of the evolution of GMSL during the LIG. In particular, at the Seychelles, we observe three pulses of RSL rise that are punctuated by ephemeral drops in RSL that expose the surface of the reef. These brief episodes of RSL fall occur so quickly that the age of corals growing immediately before and after this interruption to reef growth have overlapping analytical uncertainties. Our best estimate is that the first ephemeral RSL fall at the Seychelles occurred within 500 years, indicating rapid rates of sea level fall and rise superimposed on a longer-term trend of rising seas. While our  $^{230}\text{Th}$ -ages coupled with reef sedimentology and stratigraphy help to define the timing and nature of GMSL change during the LIG, the relatively high elevations of peak RSL in the Seychelles remain difficult to

reconcile with RSL observations in the Bahamas that seem to imply a lower GMSL (8, 12, 54).

The temporal offset in peak insolation in the Northern and Southern Hemispheres during the LIG and resulting asynchronous contribution of the Greenland and Antarctic ice sheets is notably different than anthropogenic greenhouse warming that warms both poles simultaneously, driving contemporaneous polar ice sheet retreat in both hemispheres. The masking of the contribution of individual ice sheets to LIG sea level rise due to out-of-phase growth and decay of polar ice sheets during the LIG suggests that the individual ice sheets may be more sensitive to warming than previously inferred from far-field sea level estimates that relied on quantifying ice sheet contributions at the time that peak GMSL was attained. Hence, our observation of episodic reef growth driven by out-of-phase contributions from polar ice sheets during the LIG is directly relevant to future sea level rise projections. Put simply, peak GMSL during the LIG may only represent a lower bound estimate of total future sea level rise under global warming conditions given that both poles will be contributing simultaneously.

## MATERIALS AND METHODS

### Experimental design

This work was conducted in four phases: fieldwork, analysis of field data, laboratory work, followed by analysis of laboratory data. During the fieldwork phase, we identified outcrops with in situ corals within a framework that could provide information about the past position of sea level. We documented the outcrops using imagery, surveying, and detailed descriptions of the sedimentary and stratigraphic observations including identification of floral and faunal elements. All samples were placed into an elevation reference frame relative to the local tidal datum. During the second phase of the project, these field observations were analyzed to provide interpretations of corals assemblages, stratigraphic relationships, and paleowater depth. The third phase of the project included assessment of coral preservation using visual inspection and x-ray diffraction to assess the mineralogy. A subset of the samples passing this screening process were dated using U-series measurements. The final step involved analysis of the laboratory-derived data. Details of the methods for each of these steps are provided below.

### Surveying

Coral elevations for all sites except 4 and 19A were taken at the uppermost surface of corals in the growth position using a Leica GS14 differential GPS system in combination with a Leica TS02 Plus total station with uncertainties ranging from 0.1 to 0.4 m. Sites 4 and 19A were surveyed using a total station with optical level and graduated staff as described in (9). Outcrop elevations with respect to a tidal datum were determined by comparing a series of 10-min water level measurements from an elevation-surveyed HOBO U20 water level data logger to the tide gauge record at Point La Rue, Mahé for which tidal datums have been previously determined. The water level data was then compared to a static GPS measurement at the site of the water logger. From this process, we could determine MSL with respect to a model geoid [EGM2008 (75)] on each island and thus with respect to each outcrop on an island. We report all elevations relative to MSL.

The elevations of the two highest corals are reported as  $7.4 \pm 0.1$  m (site 7) and  $7.4 \pm 0.2$  m (site 11) (data S1). We note that the highest

observed in situ coral in the Seychelles (from site 7) was previously reported at  $8.0 \pm 0.2$  m (9). Subsequently, a 40-cm discrepancy was found in the field notes for the elevation survey of site 7, in comparison to a later GPS survey of the same outcrop. We also report elevations here relative to MSL rather than mean low water springs (MLWS), which lowers the reported elevation by 0.2 m. Hence, this elevation has been revised to the value reported here,  $7.4 \pm 0.1$  m. As described in (32), an elevation correction of  $-1.05$  m was applied to the corals from Grand Anse (site 11), which is located on the south-east coast of La Digue. This is because we were initially unable to reference our elevation measurements at Grand Anse to MSL due to the rough swell on this side of the island that is exposed to the southeast trade winds and have since corrected it. This correction is further described in (32).

### Paleowater depth

Paleowater depth estimates were made for each sample based on the coral assemblage analysis detailed in (32) and shown in Fig. 2. Four assemblages observed in the fossil reef outcrops were defined and paleowater depth estimates assigned based on the local modern distributions of those corals. We further narrow any paleowater depth estimates to local modern counterparts, which are observed in the back-reef and lagoon between 0 and 2 m below MSL as the samples dated here are derived from the most landward extent of the LIG reef.

### X-ray diffraction

Corals were assessed for preservation of original aragonite mineralogy (data S2) using techniques described in detail elsewhere (76) and briefly summarized here. Measurements were made on a Rigaku Ultima IV with a Copper K $\alpha$  tube. Low-Mg (LMC) and high-Mg calcite (HMC) quantities were estimated using a weighted least squares linear model for concentrations between 0 and 5%, and a spline model for calcite concentrations above 5% at the 95% confidence interval (CI). Limits of quantification for this technique are 2.2 and 0.5% for LMC and HMC, respectively (76). Based on these limits, samples with less than 2.2% total calcite were selected for subsequent  $^{230}\text{Th}$  dating. Three samples with total calcite slightly greater than 2.2% were selected for dating to target a particular stratigraphic interval because the uncertainties were large due to the calibration procedure (76). Subsequent geochemical data showed two of them to be too altered for inclusion in the final age dataset, and they were stratigraphically inverted relative to the rest of the data set.

### $^{230}\text{Th}$ dating

Twenty-four corals that passed the XRD screening were subsampled into chips and dated in triplicate (separate subsamples) on one of two multicollector inductively coupled plasma mass spectrometers (Thermo-Scientific Neptune or Neptune Plus) at the Minnesota Isotope Laboratory (fig. S7). The chemical procedures used to separate U and Th for dating are as described in (28). For 15 samples measured on the Neptune, U and Th isotopes were measured on Faraday cups and a MasCom multiplier behind a retarding potential quadrupole according to protocols described in (77). For the nine samples measured on the Neptune Plus, all U and Th isotopes were measured on Faraday cups with protocol similar to (77), but with  $^{234}\text{U}$  and  $^{230}\text{Th}$  measured on a Faraday cup with a  $10^{13}$ -ohm resistor. We have reported all the geochemical data according to the data-reporting standards outlined in (78) (data S1). The data were first evaluated for detrital Th contamination, and subsamples with  $^{230}\text{Th}/^{232}\text{Th}$  activity

ratios  $<500$  were screened out. We also screened out measurements that have  $\delta^{234}\text{U}_i$  values  $>5\%$  away from the value of modern seawater (145‰) (79). Four coral ages that were stratigraphically out of order were also screened out (fig. S7 and data S3).  $^{230}\text{Th}$  dates were computed using a bulk crustal composition to derive Th-corrected ages. Given the low concentrations of detrital Th, this has an insignificant effect on the reported age. Corals with nonreproducible ages were also screened out (i.e., subsamples that did not have ages within error of each other). These criteria for detecting diagenesis in coral samples are well described (9, 27, 79–81), and a total of nine corals, of the 24 corals dated, were screened out on the basis of one or more of these criteria (data S3). After the data for all the individual subsamples were screened, we computed inverse-variance-weighted means of the ages for each coral. Changing these screening parameters does not change the primary observations of the dataset or the estimates on the timing of the transitions between reef growth.

Three modern *Pocillopora damicornis* specimens from the Seychelles were analyzed, yielding an average  $\delta^{234}\text{U}$  value of  $145.3 \pm 1.5\%$ , which is in agreement with the global average modern coral composition ( $145.0 \pm 1.5\%$ ) (79). A comparison of the unscreened  $\delta^{234}\text{U}_i$  values from this study and those published by Dutton *et al.* and Israelson *et al.* (9, 33) that were generated in a different laboratory reveals an apparent offset of a few permil between the two datasets, which both contain corals from some of the same outcrops (fig. S8). This apparent systematic offset prompted us to investigate the potential for a bias in the U-series data resulting from different calibration techniques used in the laboratories: gravimetric at the Minnesota Isotope Laboratory (77) versus secular equilibrium (HU-1) at The Australian National University (ANU) (9). Analysis of the ANU HU-1 standard at the Minnesota Isotope Laboratory showed that the  $[\text{}^{230}\text{Th}/\text{}^{238}\text{U}]$  is  $0.9992 \pm 0.00057$  and the  $[\text{}^{234}\text{U}/\text{}^{238}\text{U}]$  is  $0.99861 \pm 0.00057$  ( $\delta^{234}\text{U}$  value is  $-1.39 \pm 0.57\%$ ) (table S3). Because both of these activity ratios are slightly less than 1, it makes a negligible ( $\sim 0.02$  ka) difference to the ages reported in (9) but does change the back-calculated  $\delta^{234}\text{U}_i$  value of the samples analyzed at The ANU, reducing it by a couple permil and hence removing the bias originally noted between the two datasets (fig. S8). Therefore, we normalized all of the data from the ANU laboratory using the measured value for HU-1 at Minnesota so that the two datasets could be integrated. The coral  $^{230}\text{Th}$  measurements that were measured in other laboratories that are plotted in Fig. 3 for comparison to the Seychelles data have all been normalized to the same decay constants and have taken account of interlaboratory spike calibrations between laboratories as explained in (27).

### Timing of reef growth

Duration of reef growth was defined by the ages of the first and last corals within a stratigraphic reef unit (table S4). In some cases, multiple ages were averaged together where data from multiple outcrops was used to constrain the timing of the three episodes of reef growth (reefs A to C). The discontinuity separating reef A from reef B was identified within all the dated outcrops. The overlapping uncertainties on ages from the top of reef A and the bottom of reef B indicate that the process giving rise to the discontinuity occurred rapidly, potentially within less than 500 years (based on the difference between the bounding ages) or up to 1.5 kyr if the total range of uncertainty is considered. Given the reproducibility of the accuracy of the timing of reef growth between different outcrops, the former estimate is more likely. The timing of the discontinuity between reefs B

and C is not as well constrained due to pervasive alteration of the corals in the uppermost portion of reef B in all the dated outcrops.

### GMSL and rates of sea level rise

The focus of the present study is to assess the timing of reef growth, including the timing of peak RSL in the Seychelles. A robust assessment of the magnitude and rates of GMSL during the LIG using the combined Seychelles dataset would require further GIA modeling including scenarios involving various contributions from the AIS, GIS, and LIS that is beyond the scope of this manuscript but remains an important target for future work. Here, we discuss some important considerations for the relation between RSL and GMSL at this site and describe the method used to convert the data to GMSL shown in Fig. 3 as an illustration of an example of what the Seychelles coral data might mean for rates of GMSL rise.

While no region is entirely immune to deformation of the solid earth and gravity field, numerical models predict that GIA corrections to RSL for GMSL estimates will be relatively small in the Seychelles (8, 29, 30). We take the highest coral ( $7.4 \pm 0.1$  m) to represent peak RSL at  $122.8 \pm 0.5$  ka. To estimate the GMSL signal, we use the ice-age GIA correction from two different GIA predictions, one showing a fairly constant offset between RSL and GMSL, and the second that has a small but changing offset between RSL and GMSL across the interglacial (fig. S5) (8, 82). Both cases depict a forward model where GMSL is held constant at 0 m (equal to present day GMSL) without a contribution from the fingerprint of polar ice sheets that contributed to the highstand. We then correct the Seychelles RSL data to convert the signal to inferred GMSL (Fig. 3 and fig. S6). We note that adding the fingerprint for meltwater derived from ice sheets during the LIG would slightly lower the GMSL estimates provided here but by less than a meter. This exercise illustrates that despite the differences in predicted RSL between these simulations, to achieve the rising RSL observed in the Seychelles between 129 and 122 ka would require a rise in GMSL across this time interval as well. Similarly, at another far-field site, the relatively stable elevations of the highest corals in Western Australia across the same time interval would also require a rise in GMSL (Fig. 3). While the rate of GMSL rise in both of these far-field sites will depend on the specifics of the GIA model and parameters, the recognition that there must have been a net rise in GMSL across this time interval can be used to test other reconstructions of GMSL change during the LIG.

We highlight that the GMSL trends shown in Fig. 3 for the Seychelles and Western Australia do not include the fingerprint of high-latitude ice sheet contributions during the interglacial that would lower the absolute elevation of inferred GMSL and hence should not be used as an interpretation of LIG GMSL without this contribution factored in. For example, to infer peak GMSL, we note that RSL in the Seychelles is projected to underestimate GMSL by an estimated 0.3 to 1.1 m at 123 ka, depending on the GIA model used (fig. S6). Retreat of the polar ice sheets during the interglacial using the Seychelles coral elevations that have been corrected for the “ice-age” GIA signal would lead to an overestimation of the magnitude of peak GMSL by an amount dependent on the relative contributions of the Greenland, Antarctic (and potentially Laurentide) ice sheets during the interglacial (29). Using a matrix of combinations of possible contributions for additional meltwater during the interglacial, the net effect of the ice-age GIA contribution and the fingerprint of meltwater during the interglacial is a peak GMSL that is between 0.3 and 1.4 m lower than the 7.4 m observed RSL peak in the Seychelles

(fig. S6). These scenarios are shown as possible interpretations using a range of previously published GIA and ice sheet models to illustrate that the assumptions within these models about the magnitude, timing, and source of meltwater ultimately determine the conclusion about absolute elevation of GMSL at any point during the interglacial.

Ignoring the abrupt changes in RSL that interrupted reef growth at 126 and 124 ka, we calculate a background rate of GMSL rise using the two GIA predictions noted above using a least-squares fit that accounts for uncertainty in both age and elevation of the screened, inverse-variance-weighted means of each coral. The closed-system, shallow-facies, sea level record presented here shows RSL at  $5.7 \pm 0.2$  m early during the LIG at  $128.7 \pm 0.5$  ka with an overall rise of  $0.32 \pm 0.3$  m/kyr to  $7.4 \pm 0.2$  m at  $122.8 \pm 0.5$  ka. We calculate a GMSL rise rate of  $0.29 \pm 0.03$  m/kyr using GIA corrected elevations following the model predictions of (8). Using an alternative GIA model scenario [the LAM ice model in (82)], rates of sea level rise are higher, averaging about twice as fast ( $\sim 0.62$  m/kyr) (fig. S6A).

### Comparison to other coral data

To create the panels in Figure 3 representing the coral age-elevation data from Western Australia, Bahamas, and Barbados, we used data that have been recalculated to the same set of decay constants for  $^{234}\text{U}$  and  $^{230}\text{Th}$  (79) as reported in (27). We then screened the data at these three sites to exclude measurements with  $>2$  parts per billion detrital Th ( $^{232}\text{Th}$ ) and initial  $\delta^{234}\text{U}$  values  $>5\%$  away from modern seawater (145‰) (79) in keeping with the procedure used in (8), except for the Bahamas data that use a 10‰ window. This relaxed tolerance was adapted for the Bahamian dataset because the 5‰ criterion screened out most of the data. The result in the timing between the two reefs is the same in these two scenarios (5 or 10‰) but is easier to see with the larger dataset using the relaxed screening criterion.

To illustrate examples of how accounting for GIA corrections would affect the inferred GMSL signal, we applied GIA corrections to the Seychelles and Western Australia datasets as described above. The Barbados record was not adjusted to a GMSL scale since the GIA-correction is larger at this site and more sensitive to GIA model parameters [e.g., (8, 83)]. The reconstructed absolute elevations of the Barbados samples are also sensitive to uplift rates and reported elevations, both of which have uncertainties of at least several meters.

### Statistical methods

We used an inverse-variance weighted mean to calculate the mean age of each coral from multiple subsamples that were dated. To estimate a rate of GMSL rise implied from our data (not including the sea level changes at the discontinuities), we first applied the GIA corrections and then used a least-squares fit to account for uncertainty in both elevation and age (as represented by the inverse-variance-weighted mean).

### Supplementary Materials

#### The PDF file includes:

Supplementary Text  
Figs. S1 to S8  
Tables S1 to S4  
Legends for data S1 to S3  
References

#### Other Supplementary Material for this manuscript includes the following:

Data S1 to S3

## REFERENCES AND NOTES

- A. Dutton, A. E. Carlson, A. J. Long, G. A. Milne, P. U. Clark, R. DeConto, B. P. Horton, S. Rahmstorf, M. E. Raymo, Sea-level rise due to polar ice-sheet mass loss during past warm periods. *Science* **349**, aaa4019 (2015).
- A. Govin, E. Capron, P. C. Tzedakis, S. Verheyden, B. Ghaleb, C. Hillaire-Marcel, G. St-Onge, J. S. Stoner, F. Bassinot, L. Bazin, T. Blunier, N. Combourieu-Nebout, A. El Ouahabi, D. Genty, R. Gersonde, P. Jimenez-Amat, A. Landais, B. Martrat, V. Masson-Delmotte, F. Parrenin, M. S. Seidenkrantz, D. Veres, C. Waelbroeck, R. Zahn, Sequence of events from the onset to the demise of the Last Interglacial: Evaluating strengths and limitations of chronologies used in climatic archives. *Quat. Sci. Rev.* **129**, 1–36 (2015).
- J. S. Hoffman, P. U. Clark, A. C. Parnell, F. He, Regional and global sea-surface temperatures during the last interglaciation. *Science* **355**, 276–279 (2017).
- J. Jouzel, V. Masson-Delmotte, O. Cattani, G. Dreyfus, S. Falourd, G. Hoffmann, B. Minster, J. Nouet, J. M. Barnola, J. Chappellaz, H. Fischer, J. C. Gallet, S. Johnsen, M. Leuenberger, L. Loulergue, D. Luthi, H. Oerter, F. Parrenin, G. Raisbeck, D. Raynaud, A. Schilt, J. Schwander, E. Selmo, R. Souchez, R. Spahni, B. Stauffer, J. P. Steffensen, B. Stenni, T. F. Stocker, J. L. Tison, M. Werner, E. W. Wolff, Orbital and millennial antarctic climate variability over the past 800,000 years. *Science* **317**, 793–796 (2007).
- NEEM community members, Eemian interglacial reconstructed from a Greenland folded ice core. *Nature* **493**, 489–494 (2013).
- L. C. Sime, E. W. Wolff, K. I. Oliver, J. C. Tindall, Evidence for warmer interglacials in East Antarctic ice cores. *Nature* **462**, 342–345 (2009).
- B. Stenni, V. Masson-Delmotte, E. Selmo, H. Oerter, The deuterium excess records of EPICA Dome C and Dronning Maud Land ice cores (East Antarctica). *Quat. Sci. Rev.* **29**, 146–159 (2010).
- A. Dutton, K. Lambeck, Ice volume and sea level during the Last Interglacial. *Science* **337**, 216–219 (2012).
- A. Dutton, J. M. Webster, D. Zwart, K. Lambeck, B. Wohlfarth, Tropical tales of polar ice: Evidence of Last Interglacial polar ice sheet retreat recorded by fossil reefs of the granitic Seychelles islands. *Quat. Sci. Rev.* **107**, 182–196 (2015).
- R. Kopp, F. Simons, J. Mitrovica, A. Maloof, M. Oppenheimer, Probabilistic assessment of sea level during the last interglacial stage. *Nature* **462**, 863–867 (2009).
- B. Dyer, J. Austermann, W. J. D'Andrea, R. C. Creel, M. R. Sandstrom, M. Cashman, A. Rovere, M. E. Raymo, Sea-level trends across The Bahamas constrain peak last interglacial ice melt. *Proc. Natl. Acad. Sci. U.S.A.* **118**, e2026839118 (2021).
- O. A. Dumitru, B. Dyer, J. Austermann, M. R. Sandstrom, S. L. Goldstein, W. J. D'Andrea, M. Cashman, R. Creel, L. Bolge, M. E. Raymo, Last interglacial global mean sea level from high-precision U-series ages of Bahamian fossil coral reefs. *Quat. Sci. Rev.* **318**, 108287 (2023).
- J. Austermann, J. X. Mitrovica, P. Huybers, A. Rovere, Detection of a dynamic topography signal in last interglacial sea-level records. *Sci. Adv.* **3**, e1700457 (2017).
- R. M. DeConto, D. Pollard, R. B. Alley, I. Velicogna, E. Gasson, N. Gomez, S. Sadai, A. Condron, D. M. Gilford, E. L. Ashe, R. E. Kopp, D. Li, A. Dutton, The Paris climate agreement and future sea-level rise from Antarctica. *Nature* **593**, 83–89 (2021).
- J. Chen, H. Curran, B. White, G. Wasserburg, Precise chronology of the last interglacial period: 234U-230Th data from fossil coral reefs in the Bahamas. *Bull. Geol. Soc. Am.* **103**, 82–97 (1991).
- R. E. Kopp, F. J. Simons, J. X. Mitrovica, A. C. Maloof, M. Oppenheimer, A probabilistic assessment of sea level variations within the last interglacial stage. *Geophys. J. Int.* **193**, 711–716 (2013).
- M. J. O'Leary, P. J. Hearty, W. G. Thompson, M. E. Raymo, J. X. Mitrovica, J. M. Webster, Ice sheet collapse following a prolonged period of stable sea level during the last interglacial. *Nat. Geosci.* **6**, 796–800 (2013).
- E. J. Rohling, F. D. Hibbert, K. M. Grant, E. V. Galaasen, N. Irvani, H. F. Kleiven, G. Marino, U. Ninnemann, A. P. Roberts, Y. Rosenthal, H. Schulz, F. H. Williams, J. Yu, Asynchronous Antarctic and Greenland ice-volume contributions to the last interglacial sea-level highstand. *Nat. Commun.* **10**, 5040 (2019).
- P. Blanchon, A. Eisenhauer, J. Fietzke, V. Liebetrau, Rapid sea-level rise and reef back-stepping at the close of the last interglacial highstand. *Nature* **458**, 881–884 (2009).
- P. Hearty, J. Hollin, A. Neumann, M. O'Leary, M. McCulloch, Global sea-level fluctuations during the Last Interglaciation (MIS 5e). *Quat. Sci. Rev.* **26**, 2090–2112 (2007).
- W. G. Thompson, S. L. Goldstein, Open-system coral ages reveal persistent subsorbital sea-level cycles. *Science* **308**, 401–404 (2005).
- W. G. Thompson, H. A. Curran, M. A. Wilson, B. White, Sea-level and ice-sheet instability during the Last Interglacial: New Bahamas evidence. *Nat. Geosci.* **4**, 684–687 (2011).
- W. Thompson, H. Curran, M. Wilson, Sea-level oscillations during the last interglacial highstand recorded by Bahamas corals. *Nat. Geosci.* **4**, 684–687 (2011).
- N. L. M. Barlow, E. L. McClumty, P. L. Whitehouse, C. R. Stokes, S. S. R. Jamieson, S. A. Woodroffe, M. J. Bentley, S. L. Callard, C. Ó. Cofaigh, D. J. A. Evans, J. R. Horrocks, J. M. Lloyd, A. J. Long, M. Margold, D. H. Roberts, M. L. Sanchez-Montes, Lack of evidence for a substantial sea-level fluctuation within the Last Interglacial. *Nat. Geosci.* **11**, 627–634 (2018).
- V. J. Polyak, B. P. Onac, J. J. Fornós, C. Hay, Y. Asmerom, J. A. Dorale, J. Ginés, P. Tuccimei, A. Ginés, A highly resolved record of relative sea level in the western Mediterranean Sea during the last interglacial period. *Nat. Geosci.* **11**, 860–864 (2018).
- C. H. Stirling, T. M. Esat, K. Lambeck, M. T. McCulloch, Timing and duration of the Last Interglacial: Evidence for a restricted interval of widespread coral reef growth. *Earth Planet. Sci. Lett.* **160**, 745–762 (1998).
- F. D. Hibbert, E. J. Rohling, A. Dutton, F. H. Williams, P. M. Chutcharavan, C. Zhao, M. E. Tamisiea, Coral indicators of past sea-level change: A global repository of U-series dated benchmarks. *Quat. Sci. Rev.* **145**, 1–56 (2016).
- R. L. Edwards, J. H. Chen, T.-L. Ku, G. J. Wasserburg, Precise timing of the last interglacial period from mass spectrometric determination of thorium-230 in corals. *Science* **236**, 1547–1553 (1987).
- C. Hay, J. X. Mitrovica, N. Gomez, J. R. Creveling, J. Austermann, R. E. Kopp, The sea-level fingerprints of ice-sheet collapse during interglacial periods. *Quat. Sci. Rev.* **87**, 60–69 (2014).
- G. A. Milne, J. X. Mitrovica, Searching for eustasy in deglacial sea-level histories. *Quat. Sci. Rev.* **27**, 2292–2302 (2008).
- Y. Mart, The tectonic setting of the Seychelles, Mascarene and Amirante plateaus in the western equatorial Indian Ocean. *Mar. Geol.* **79**, 261–274 (1988).
- K. Vyverberg, B. Dechnik, A. Dutton, J. M. Webster, D. Zwart, R. W. Portell, Episodic reef growth in the granitic Seychelles during the Last Interglacial: Implications for polar ice sheet dynamics. *Mar. Geol.* **399**, 170–187 (2018).
- C. Israelson, B. Wohlfarth, Timing of the last-interglacial high sea level on the Seychelles Islands, Indian Ocean Peer reviewed article. *Quat. Res.* **51**, 306–316 (1999).
- A. Skrivaneck, J. Li, A. Dutton, Relative sea-level change during the Last Interglacial as recorded in Bahamian fossil reefs. *Quat. Sci. Rev.* **200**, 160–177 (2018).
- R. Speed, H. Cheng, Evolution of marine terraces and sea level in the last interglacial, Cave Hill, Barbados. *Geol. Soc. Am. Bull.* **116**, 219–232 (2004).
- E. Colville, A. Carlson, B. Beard, R. Hatfield, J. S. Stoner, A. V. Reyes, D. J. Ullman, Sr-Nd-Pb isotope evidence for ice-sheet presence on Southern Greenland during the last interglacial. *Science* **333**, 620–623 (2011).
- M. M. Helsen, W. J. van de Berg, R. S. W. Van De Wal, M. R. van den Broeke, J. Oerlemans, Coupled regional climate-ice-sheet simulation shows limited Greenland ice loss during the Eemian. *Clim. Past* **9**, 1773–1788 (2013).
- E. J. Stone, D. J. Lunt, J. D. Annan, J. C. Hargreaves, Quantification of the Greenland ice sheet contribution to Last Interglacial sea level rise. *Clim. Past* **9**, 621–639 (2013).
- A. M. Yau, M. L. Bender, A. Robinson, E. J. Brook, Reconstructing the last interglacial at Summit, Greenland: Insights from GISP2. *Proc. Natl. Acad. Sci. U.S.A.* **113**, 9710–9715 (2016).
- J. Laskar, P. Robutel, F. Joutel, M. Gastineau, A. C. M. Correia, B. Lestrade, A long-term numerical solution for the insolation quantities of the Earth. *Astron. Astrophys.* **428**, 261–285 (2004).
- J. Imbrie, J. Z. Imbrie, Modeling the climatic response to orbital variations. *Science* **207**, 943–953 (1980).
- R. S. Nerem, B. D. Beckley, J. T. Fasullo, B. D. Hamlington, D. Masters, G. T. Mitchum, Climate-change-driven accelerated sea-level rise detected in the altimeter era. *Proc. Natl. Acad. Sci. U.S.A.* **115**, 2022–2025 (2018).
- A. N. Sommers, B. L. Otto-Bliesner, W. H. Lipscomb, M. Lofverstrom, S. L. Shafer, P. J. Bartlein, E. C. Brady, E. Kluzek, G. Leguy, K. Thayer-Calder, R. A. Tomas, Retreat and regrowth of the Greenland Ice sheet during the last interglacial as simulated by the CESM2-CISM2 coupled climate-ice sheet model. *Paleoceanogr. Paleoclimatol.* **36**, e2021PA004272 (2021).
- E. Capron, A. Govin, E. J. Stone, V. Masson-Delmotte, S. Mulitza, B. Otto-Bliesner, T. L. Rasmussen, L. C. Sime, C. Waelbroeck, E. W. Wolff, Temporal and spatial structure of multi-millennial temperature changes at high latitudes during the Last Interglacial. *Quat. Sci. Rev.* **103**, 116–133 (2014).
- R. M. DeConto, D. Pollard, Contribution of Antarctica to past and future sea-level rise. *Nature* **531**, 591–597 (2016).
- N. R. Golledge, P. U. Clark, F. He, A. Dutton, C. S. M. Turney, C. J. Fogwill, T. R. Naish, R. H. Levy, R. M. McKay, D. P. Lowry, N. A. N. Bertler, G. B. Dunbar, A. E. Carlson, Retreat of the Antarctic ice sheet during the last interglaciation and implications for future change. *Geophys. Res. Lett.* **48**, e2021GL094513 (2021).
- D. Lüthi, M. Le Floch, B. Bereiter, T. Blunier, J.-M. Barnola, U. Siegenthaler, D. Raynaud, J. Jouzel, H. Fischer, K. Kawamura, T. F. Stocker, High-resolution carbon dioxide concentration record 650,000–800,000 years before present. *Nature* **453**, 379–382 (2008).
- L. Loulergue, A. Schilt, R. Spahni, V. Masson-Delmotte, T. Blunier, B. Lemieux, J.-M. Barnola, D. Raynaud, T. F. Stocker, J. Chappellaz, Orbital and millennial-scale features of atmospheric CH<sub>4</sub> over the past 800,000 years. *Nature* **453**, 383–386 (2008).

49. V. Masson-Delmotte, B. Stenni, T. Blunier, O. Cattani, J. Chappellaz, H. Cheng, G. Dreyfus, R. L. Edwards, S. Falourd, A. Govin, K. Kawamura, S. Johnsen, J. Jouzel, A. Landais, B. Lemieux-Dudon, A. Lourantou, G. Marshall, B. Minster, M. Mudelsee, K. Pol, R. Rothlisberger, E. Selmo, C. Waelbroeck, Abrupt change of Antarctic moisture origin at the end of Termination II. *Proc. Natl. Acad. Sci. U.S.A.* **107**, 12091–12094 (2010).
50. H. Cheng, R. L. Edwards, A. Sinha, C. Spotl, L. Yi, S. Chen, M. Kelly, G. Kathayat, X. Wang, X. Li, X. Kong, Y. Wang, Y. Ning, H. Zhang, The Asian monsoon over the past 640,000 years and ice age terminations. *Nature* **534**, 640–646 (2016).
51. N. Irvani, U. S. Ninnemann, H. F. Kleiven, E. V. Galaasen, A. Morley, Y. Rosenthal, Evidence for regional cooling, frontal advances, and East Greenland Ice Sheet changes during the demise of the last interglacial. *Quat. Sci. Rev.* **150**, 184–199 (2016).
52. P. C. Tzedakis, R. N. Drysdale, V. Margari, L. C. Skinner, L. Menviel, R. H. Rhodes, A. S. Taschetto, D. A. Hodell, S. J. Crowhurst, J. C. Hellstrom, A. E. Fallick, J. O. Grimalt, J. F. McManus, B. Martrat, Z. Mokeddem, F. Parrenin, E. Regattieri, K. Roe, G. Zanchetta, Enhanced climate instability in the North Atlantic and Southern Europe during the last interglacial. *Nat. Commun.* **9**, 4235 (2018).
53. G. Marino, E. J. Rohling, L. Rodriguez-Sanz, K. M. Grant, D. Heslop, A. P. Roberts, J. D. Stanford, J. Yu, Bipolar seesaw control on last interglacial sea level. *Nature* **522**, 197–201 (2015).
54. P. U. Clark, F. He, N. R. Golledge, J. X. Mitrovica, A. Dutton, J. S. Hoffman, S. Dendy, Oceanic forcing of penultimate deglacial and last interglacial sea-level rise. *Nature* **577**, 660–664 (2020).
55. C. S. M. Turney, C. J. Fogwill, N. R. Golledge, N. P. McKay, E. van Sebille, R. T. Jones, D. Etheridge, M. Rubino, D. P. Thornton, S. M. Davies, C. B. Ramsey, Z. A. Thomas, M. I. Bird, N. C. Munksgaard, M. Kohno, J. Woodward, K. Winter, L. S. Weyrich, C. M. Rootes, H. Millman, P. G. Albert, A. Rivera, T. van Ommen, M. Curran, A. Moy, S. Rahmstorf, K. Kawamura, C. D. Hillenbrand, M. E. Weber, C. J. Manning, J. Young, A. Cooper, Early Last Interglacial ocean warming drove substantial ice mass loss from Antarctica. *Proc. Natl. Acad. Sci. U.S.A.* **117**, 3996–4006 (2020).
56. R. L. Barnett, J. Austermann, B. Dyer, M. W. Telfer, N. L. M. Barlow, S. J. Boulton, A. S. Carr, R. C. Creel, Constraining the contribution of the Antarctic Ice Sheet to Last Interglacial sea level. *Sci. Adv.* **9**, ead0198 (2023).
57. E. Brouard, M. Roy, P.-M. Godbout, J. J. Veillette, A framework for the timing of the final meltwater outbursts from glacial Lake Agassiz-Ojibway. *Quat. Sci. Rev.* **274**, 107269 (2021).
58. Y. Zhou, J. F. McManus, Extensive evidence for a last interglacial Laurentide outburst (L1LO) event. *Geology* **50**, 934–938 (2022).
59. A. Zhuravleva, H. A. Bauch, N. Van Nieuwenhove, Last Interglacial (MIS5e) hydrographic shifts linked to meltwater discharges from the East Greenland margin. *Quat. Sci. Rev.* **164**, 95–109 (2017).
60. E. V. Galaasen, U. S. Ninnemann, N. Irvani, H. F. Kleiven, Y. Rosenthal, C. Kissel, D. A. Hodell, Rapid reductions in North Atlantic deep water during the peak of the last interglacial period. *Science* **343**, 1129–1132 (2014).
61. J. A. L. Nicholl, D. A. Hodell, B. D. A. Naafs, C. Hillaire-Marcel, J. E. T. Channell, O. E. Romero, A Laurentide outburst flooding event during the last interglacial period. *Nat. Geosci.* **5**, 901–904 (2012).
62. J. E. N. Veron, *Coralals of the World* (Australian Institute of Marine Science, 2000).
63. G. Schellmann, U. Radtke, A revised morpho- and chronostratigraphy of the Late and Middle Pleistocene coral reef terraces on Southern Barbados (West Indies). *Earth Sci. Rev.* **64**, 157–187 (2004).
64. M. Stein, G. Wasserburg, P. Aharon, J. Chen, Z. Zhu, A. Bloom, J. Chappell, TIMS U-series dating and stable isotopes of the last interglacial event in Papua New Guinea. *Geoch. Cosmochim. Acta* **57**, 2541–2554 (1993).
65. K. Lambeck, A. Purcell, A. Dutton, The anatomy of interglacial sea levels: The relationship between sea levels and ice volumes during the Last Interglacial. *Earth Planet. Sci. Lett.* **315–316**, 4–11 (2012).
66. B. White, A. Curran, M. A. Wilson, Bahamian coral reefs yield evidence of a brief sea-level lowstand during the last interglacial. *Carbonates Evaporites* **13**, 10–22 (1998).
67. M. A. Wilson, H. A. Curran, B. White, Paleontological evidence of a brief global sea-level event during the last interglacial. *Lethaia* **31**, 241–250 (1998).
68. B. B. Whitney, J. V. Hengesh, Geomorphological evidence for late Quaternary tectonic deformation of the Cape Region, coastal west central Australia. *Geomorphology* **241**, 160–174 (2015).
69. G. E. Moseley, P. L. Smart, D. A. Richards, D. L. Hoffmann, Speleothem constraints on marine isotope stage (MIS) 5 relative sea levels, Yucatan Peninsula, Mexico. *J. Quat. Sci.* **28**, 293–300 (2013).
70. P. Clark, A. Dyke, J. Shakun, A. Carlson, J. Clark, B. Wohlfarth, J. Mitrovica, S. Hostetler, A. McCabe, The last glacial maximum. *Science* **325**, 710 (2009).
71. L. Menviel, E. Capron, A. Govin, A. Dutton, L. Tarasov, A. Abe-Ouchi, R. Drysdale, P. L. Gibbard, L. J. Gregoire, F. He, R. F. Ivanovic, M. Kageyama, K. Kawamura, A. Landais, B. Otto-Bliesner, I. Oyabu, C. Tzedakis, E. W. Wolff, X. Zhang, The penultimate deglaciation: Protocol for Paleoclimate Modelling Intercomparison Project (PMIP) phase 4 transient numerical simulations between 140 and 127 ka, version 1.0. *Geosci. Model Develop.* **12**, 3649–3685 (2019).
72. G. H. Miller, W. N. Mode, A. P. Wolfe, P. E. Sauer, O. Bennike, S. L. Forman, S. K. Short, T. W. Stafford, Stratified interglacial lacustrine sediments from Baffin Island, Arctic Canada: Chronology and paleoenvironmental implications. *Quat. Sci. Rev.* **18**, 789–810 (1999).
73. D. E. LeBlanc, J. D. Shakun, L. B. Corbett, P. R. Bierman, M. W. Caffee, A. J. Hidy, Laurentide Ice Sheet persistence during Pleistocene interglacials. *Geology* **51**, 496–499 (2023).
74. M. Iizuka, O. Seki, D. J. Wilson, Y. Suganuma, K. Horikawa, T. van de Fliert, M. Ikehara, T. Itaki, T. Irino, M. Yamamoto, M. Hirabayashi, H. Matsuzaki, S. Sugisaki, Multiple episodes of ice loss from the Wilkes Subglacial Basin during the Last Interglacial. *Nat. Commun.* **14**, 2129 (2023).
75. N. K. Pavlis, S. A. Holmes, S. C. Kenyon, J. K. Factor, The development and evaluation of the Earth Gravitational Model 2008 (EGM2008). *J. Geophys. Res.* **117**, B04406 (2012).
76. K. L. Vyverberg, J. M. Jaeger, A. Dutton, Quantifying detection limits and uncertainty in X-ray diffraction mineralogical assessments of biogenic carbonates. *J. Sediment. Res.* **88**, 1261–1275 (2018).
77. H. Cheng, R. L. Edwards, C. C. Shen, Improvements in  $^{230}\text{Th}$  dating,  $^{230}\text{Th}$  and  $^{234}\text{U}$  half-life values, and U–Th isotopic measurements by multi-collector inductively coupled plasma mass spectrometry. *Earth Planet. Sci. Lett.* **371–372**, 82–91 (2013).
78. A. Dutton, K. Rubin, N. McLean, J. Bowring, E. Bard, R. L. Edwards, G. M. Henderson, M. R. Reid, D. A. Richards, K. W. W. Sims, J. D. Walker, Y. Yokoyama, Data reporting standards for publication of U-series data for geochronology and timescale assessment in the earth sciences. *Quat. Geochronol.* **39**, 142–149 (2017).
79. P. M. Chutcharavan, A. Dutton, M. J. Ellwood, Seawater  $^{234}\text{U}/^{238}\text{U}$  recorded by modern and fossil corals. *Geochim. Cosmochim. Acta* **224**, 1–17 (2018).
80. A. Dutton, in *Handbook of Sea-Level Research*, I. Shennan, A. J. Long, B. P. Horton, Eds. (John Wiley & Sons, 2015), pp. 386–403.
81. R. L. Edwards, C. D. Gallup, H. Cheng, Uranium-series dating of marine and lacustrine carbonates. *Rev. Mineral Geochem.* **52**, 363–405 (2003).
82. S. Dendy, J. Austermann, J. R. Creveling, J. X. Mitrovica, Sensitivity of Last Interglacial sea-level high stands to ice sheet configuration during Marine Isotope Stage 6. *Quat. Sci. Rev.* **171**, 234–244 (2017).
83. J. Austermann, J. X. Mitrovica, K. Latychev, G. A. Milne, Barbados-based estimate of ice volume at Last Glacial Maximum affected by subducted plate. *Nat. Geosci.* **6**, 553–557 (2013).
84. P. M. Chutcharavan, A. Dutton, A global compilation of U-series-dated fossil coral sea-level indicators for the Last Interglacial period (Marine Isotope Stage 5e). *Earth Syst. Sci. Data* **13**, 3155–3178 (2021).
85. S. Barker, G. Knorr, R. L. Edwards, F. Parrenin, A. E. Putnam, L. C. Skinner, E. W. Wolff, M. Ziegler, 800,000 years of abrupt climate variability. *Science* **334**, 347–351 (2011).
86. L. Bazin, A. Landais, B. Lemieux-Dudon, H. T. M. Kele, D. Veres, F. Parrenin, P. Martinierie, C. Ritz, E. Capron, V. Lipenkov, M.-F. Loutre, D. Raynaud, B. Vinther, A. Svensson, S. O. Rasmussen, M. Severi, T. Blunier, M. Leuenberger, H. Fischer, V. Masson-Delmotte, J. Chappellaz, E. W. Wolff, An optimized multi-proxy, multi-site Antarctic ice and gas orbital chronology (AICC2012): 120–800 ka. *Clim. Past* **9**, 1715–1731 (2013).
87. C. Waelbroeck, L. Labeyrie, E. Michel, J. C. Duplessy, J. F. McManus, K. Lambeck, E. Balbon, M. Labracherie, Sea-level and deep water temperature changes derived from benthic foraminifera isotopic records. *Quat. Sci. Rev.* **21**, 295–305 (2002).
88. K. Lambeck, A. Purcell, S. Funder, K. H. Kjær, E. Larsen, P. Moller, Constraints on the Late Saalian to early Middle Weichselian ice sheet of Eurasia from field data and rebound modelling. *Boreas* **35**, 539–575 (2006).
89. F. Colleoni, C. Wekerle, J.-O. Naslund, J. Brandefelt, S. Masina, Constraint on the penultimate glacial maximum northern hemisphere ice topography ( $\approx 140\text{kyrs BP}$ ). *Quat. Sci. Rev.* **137**, 97–112 (2016).
90. J. D. Taylor, Coral reef and associated invertebrate communities (Mainly Molluscan) around Mahe, Seychelles. *Philos. Trans. R. Soc. Lond.* **254**, 129–206 (1968).
91. M. S. Lewis, Sedimentary environments and unconsolidated carbonate sediments of the fringing coral reefs of Mahé, Seychelles. *Mar. Geol.* **7**, 95–127 (1969).

**Acknowledgments:** We thank the citizens and authorities in the Seychelles who facilitated our fieldwork, including P. Samson at PetroSeychelles, the Seychelles National Parks Authority, and the Ministry of Environment and Energy. We also thank the Seychelles Bureau of Standards for granting us a permit to collect these samples. J. Curtis and J. Jaeger assisted with laboratory procedures. This is a contribution to the PALSEA and QUIGS working groups. **Funding:** This work was supported by the National Science Foundation grant 1155495 (to A.D.) and 1159040 (to A.D.); the Helen Junnik Endowment, University of Wisconsin-Madison (to A.D.); the Hanse-Wissenschaftskolleg Institute for Advanced Study (Germany) (to J.W.); and the National Science Foundation grants 1934477 and 2035080 (to R.M.D.) and 2202913 (to R.L.E.). **Author contributions:** Conceptualization: A.D., J.M.W., and K.V. Investigation: K.V., A.D., B.D., J.M.W., and D.Z. Methodology: K.V., P.Z., M.P., R.L.E., A.D., J.M.W., and R.M.D. Formal analysis: K.V., B.D.,

A.D., J.M.W., D.Z., and R.L.E. Visualization: K.V., B.D., A.D., and R.M.D. Data curation: K.V. and A.D. Validation: K.V., A.D., B.D., J.M.W., M.P., and P.Z. Supervision: A.D., J.M.W., and R.L.E. Writing—original draft: K.V. and A.D. Writing—review and editing: K.V., A.D., B.D., J.M.W., R.L.E., and R.M.D. Resources: A.D., J.M.W., and R.L.E. Funding acquisition: A.D. and R.L.E. Project administration: A.D. **Competing interests:** The authors declare that they have no competing interests. **Data and materials availability:** All data needed to evaluate the conclusions in the paper are present in the paper and/or the Supplementary Materials. Sample metadata are also archived with SESAR<sup>2</sup> ([https://app.geosamples.org/sample\\_group.php?group\\_id=443](https://app.geosamples.org/sample_group.php?group_id=443)) and the three supplementary data files are also archived at the NOAA/WDS Paleoclimate archive

([www.ncei.noaa.gov/pub/data/paleo/coral/indian\\_ocean/dutton2025/dutton2025-seychelles-s1.txt](http://www.ncei.noaa.gov/pub/data/paleo/coral/indian_ocean/dutton2025/dutton2025-seychelles-s1.txt), [www.ncei.noaa.gov/pub/data/paleo/coral/indian\\_ocean/dutton2025/dutton2025-seychelles-s2.txt](http://www.ncei.noaa.gov/pub/data/paleo/coral/indian_ocean/dutton2025/dutton2025-seychelles-s2.txt), and [www.ncei.noaa.gov/pub/data/paleo/coral/indian\\_ocean/dutton2025/dutton2025-seychelles-s3.txt](http://www.ncei.noaa.gov/pub/data/paleo/coral/indian_ocean/dutton2025/dutton2025-seychelles-s3.txt)).

Submitted 5 November 2024

Accepted 9 May 2025

Published 13 June 2025

10.1126/sciadv.adu3701